Research Article

X-ray reflectivity and X-ray photoelectron spectroscopy studies on reactively sputtered Nb_2O_5-based thin-film devices

Karimul Islam[1,2] · Rezwana Sultana[1,2] · Abhishek Rakshit[1,2] · U. K. Goutam[2] · Supratic Chakraborty[3]

Received: 18 October 2019 / Accepted: 17 March 2020 / Published online: 31 March 2020

Abstract
The reactively sputtered Nb_2O_5-based metal–oxide–semiconductor devices deposited under different O_2/Ar ratios have been studied using laboratory-based X-ray reflectivity (XRR) and synchrotron-based X-ray photoelectron spectroscopy techniques. The $I - V$ characteristics reveal a sharp transition in the magnitude of current (~ up to five orders) signifying a switching phenomenon between high-resistance and low-resistance states. The electron density profile, derived from XRR data, shows a dependence of the switching properties on the film porosity. Further, the non-lattice oxygen in the film also plays a role in determining the on/off ratio of the devices. Therefore, besides the presence of non-lattice oxygen, film porosity also influences the resistive switching behavior of the Nb_2O_5-based devices.

Keywords Reactive sputtering · Porosity · Non-lattice oxygen · Resistive switching

1 Introduction

Transition metal oxide-based resistive switching devices show their prominence in the recent times for nonvolatile memory (NVM) applications [1, 2]. Among them, high-κ dielectric materials have drawn the attention of the researchers for fabrication of NVM devices because the equivalent oxide thickness (EOT) of the gate dielectric layer can be scaled down to sub-nm dimensions. Among the high-κ elements, oxides of Hf [3], Zr [4], Ti [5], etc., have already settled their position in the NVM family. It is needless to mention that first resistive switching property of niobium oxide was observed by Hiatt et al. in 1965 [6]. Niobium (Nb) has now been considered because it offers various oxides with different physical and electrical properties [7]. Among them, NbO, NbO_2, and Nb_2O_5 are mostly studied that show metallic, semiconducting, and insulating electrical properties, respectively [8]. Having a relatively large value of dielectric constant, Nb_2O_5 is a multi-purpose oxide and has been integrated into device structures which serve widespread applications [9]. Since niobium oxide (NbO_x) films possess several interesting properties, researchers have been exploring their properties for various applications where NbO_x films have been grown/deposited using sputtering [10], plasma oxidation [11], molecular beam epitaxy [12], pulsed laser deposition [13], etc. Researchers have so far concentrated on the electrochromic properties of niobium oxides [14]. Change in refractive index and deposition stress of sputter-deposited Nb_2O_5 film has been reported recently by varying deposition pressure and oxygen content in the plasma [15]. In recent times, threshold switching properties of NbO-based metal–insulator–metal (MIM) devices have been presented [16, 17]. A multilayer NbO-based MIM structure with five-order on/off ratios is also reported [18]. There are several pending issues with NbO_x that require to be addressed.

In this communication, the niobium pentoxide films, deposited by dc reactive sputtering at different Ar/O_2

✉ Supratic Chakraborty, supratic.chakraborty@saha.ac.in; Karimul Islam, karimul.islam@saha.ac.in; Rezwana Sultana, rezwana.sultana@saha.ac.in; Abhishek Rakshit, abhishek.rakshit@saha.ac.in; U. K. Goutam, ukgoutam@rrcat.gov.in | [1]Saha Institute of Nuclear Physics, 1/AF Bidhannagar, Kolkata 700 064, India. [2]Homi Bhabha National Institute, BARC Training School Complex, Anushaktinagar, Mumbai 400 094, India. [3]Saha Institute of Nuclear Physics, 1/AF Bidhannagar, Kolkata 700 064, India.

ratios, were integrated to Al/Nb_2O_5/Si metal–oxide–semiconductor (MOS) structure to study their resistive switching properties. Grazing incidence X-ray reflectivity technique also is employed to estimate the porosity of Nb_2O_5 thin films and to correlate its role with the resistive switching properties of the devices. Further, the XPS technique is employed for elemental mapping to explain various device properties. The results are presented and discussed here.

2 Experimental

n-type Si (100) substrates having a resistivity of 0.1–0.5 Ω - cm and 1 cm × 1 cm area were used for depositing the oxide films and subsequent MOS device fabrication. Niobium oxide films were deposited by dc reactive sputtering of a 99.9% metallic niobium target in O_2/Ar plasma at room temperature. A standard protocol for cleaning silicon wafers known as the Radio Corporation of America (RCA) cleaning technique was used for removing the metallic, organic, and inorganic impurities from the substrate surface [19]. The RCA cleansing was followed by a 1-min immersion in 1% hydrofluoric (HF) acid solution for stripping off the native SiO_x layer from the silicon surface prior to loading into the sputtering chamber. After achieving a base pressure of ~ 3×10^{-6} mTorr, the deposition was carried out at a constant pressure of 5 mTorr for 40 min at 80 W dc power at different O_2/Ar ratios. The substrates were given a rotation of 30 rpm to ensure film uniformity. The sample nomenclature of the deposited films at various oxygen concentrations estimated as $\frac{O_2}{O_2+Ar}$ is listed in Table 1. The thickness and surface roughness of the as-deposited films were extracted from XRR study using a Rigaku SmartLab 3 kW, X-ray diffractometer. The energies of the primary X-ray beam (CuK_α) used in XRR were 8 keV. To determine the stoichiometry of the NbO_x films and the oxidation states of niobium as well, XPS study was carried out at X-ray Photo-Electron Spectroscopy (PES) Beamline (BL-14) of Indus-2 at RRCAT, Indore, India. The energy of

Table 1 Nomenclature of the reactively sputter-deposited niobium oxide thin films

Sample name	Ar/O_2	Oxygen concentration (%)
N1	5:1	17
N2	5:2	28
N3	3:2	40
N4	1:1	50

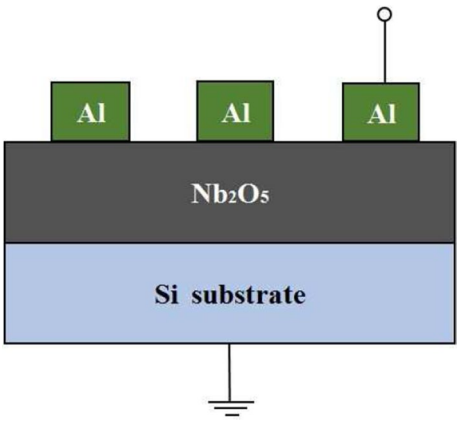

Fig. 1 A schematic diagram of Al/Nb_2O_5/Si device

Indus-2 storage ring is 2.5 GeV. The achievable base pressure of the analytical chamber is $\leq 5\times10^{-9}$ mbar, while the electron beam energy was 4.4 keV. The XPS survey scan was taken by sweeping the binding energy from 604.2 to 0 eV with a pass energy of 150 eV [20]. A 300-nm-thick aluminum metal deposition on the niobium oxide films was performed by electron beam evaporation and patterned into 100-μm-diameter gate electrodes by UV photolithography technique. Figure 1 shows the schematic diagram of Nb_2O_5-based metal–oxide–semiconductor (MOS) structures. A voltage sweep was applied to the Al gate electrodes, and the corresponding gate current was measured using a keithley-make 4200 semiconductor parameter analyzer equipped with a 4200-PA amplifiers. The substrate chuck of the Signatone probe station was maintained at room temperature during the electrical characterizations. The probe station was isolated from light and shielded electrically. Ten devices for each set of samples have been measured.

3 Results and discussion

The XRR data of the above four films deposited on Si substrate under different conditions are demonstrated in Fig. 2a. The XRR profiles were fitted using the Parratt formalism to estimate the film thickness [21]. During the Parratt fitting, the films were sectioned into multilayers such that the surface roughness and interface roughness were extracted accurately [22]. The inset of Fig. 2a displays the electron density profile (EDP) for all the samples. The mass density of Nb_2O_5 was considered during the fitting process.

The parameters extracted from the Parratt fitting of the XRR profiles are depicted in Table 2. Upon analysis, it is revealed that the thickness of N1 sample is maximum, and the film thickness follows a decreasing trend with increasing O_2 content in the reactive plasma. The

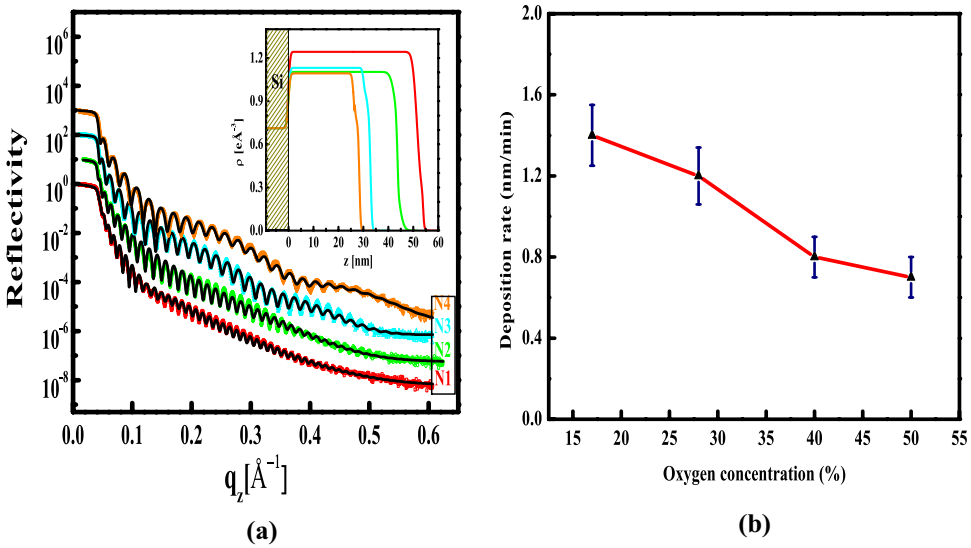

Fig. 2 **a** XRR profiles for all as-deposited samples: colored symbol indicates experimental data for different O_2 to Ar ratios. Solid black line shows the fitted data. The inset shows electron density profile of all the samples. **b** Deposition rate of Nb_2O_5 films at different O_2 concentrations. Error bars in the figure denote standard deviation

Table 2 Different thin-film parameters extracted from the XRR data

Sample name	Oxide thickness (nm)	Electron density (e Å^{-3})	Surface roughness (Å)	Oxide/Si interface roughness (Å)
N1	54.5 ± 0.2	1.2 ± 0.04	3.2 ± 0.2	6.4 ± 0.4
N2	47.5 ± 0.2	1.1 ± 0.04	2.2 ± 0.2	6.1 ± 0.4
N3	34.0 ± 0.1	1.1 ± 0.04	5.2 ± 0.4	5.4 ± 0.4
N4	29.3 ± 0.1	1.1 ± 0.04	4.3 ± 0.3	6.0 ± 0.4

sputter-deposited films at various O_2/Ar ratios show a very smooth surface with roughness ranging from 5 to 2 Å. These extremely low values are reproducible over thin film because of the advantages of the XRR technique.

Since Nb sputtering yield by Ar is more than that by O_2, the deposition rate decreases with increasing O_2 ratio in the plasma. The surface roughness also increases with O_2 plasma content. To study the top surface morphology of the films, atomic force microscopy technique has been employed using AFM(CSI, Nano-Observer). The measurements have been taken for all the samples and found that roughness data are more or less similar as obtained from GI-XRR technique. A representative AFM image of N3 sample is shown in Fig. 3. The average roughness obtained from AFM data using Gwyddion software is 6±2 Å, and the same obtained from GI-XRR data is 5±0.4 Å. The N3 film shows the highest surface roughness of ~ 5 Å. It appears from the profile that a very thin porous Nb_2O_5 film is deposited over relatively denser film at higher O_2 content in the plasma which is evident from N3 and N4 samples. Deposition rates of Nb_2O_5 film at different O_2 concentrations in the plasma are shown in Fig. 2b. A sample was deposited at 66% O_2 content in the plasma only to see its role on the deposition rate at higher concentration. It is also concluded that the deposition rate becomes nearly constant after a critical O_2 content in the reactive plasma.

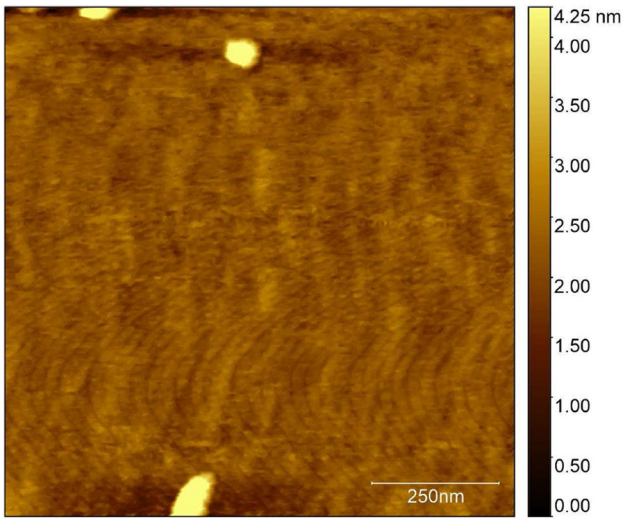

Fig. 3 AFM image of N3 sample

The deconvoluted XPS spectra of Nb 3d and O 1s for all the samples are shown in Fig. 4a and b, respectively. A software PeakFit 4.11 is used to deconvolute the XPS spectra. The deconvoluted Nb 3d spectra show two peaks

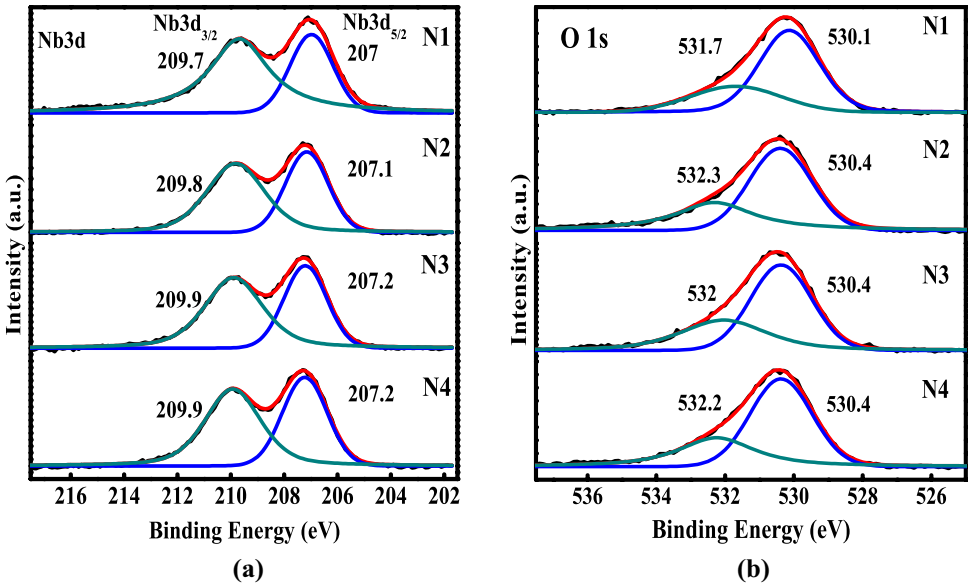

Fig. 4 XPS spectra of Nb_2O_5 films deposited at room temperature: **a** Nb 3d and **b** O 1s

Table 3 Percentage of non-lattice oxygen extracted from the XPS spectra

Sample name	Non-lattice oxygen (%)
N1	28.4 ± 0.7
N2	29.2 ± 0.3
N3	32.7 ± 0.4
N4	31.0 ± 0.1

at 207 and 209.7 eV for N1 sample denoting the Nb^{5+} $3d_{5/2}$ and $3d_{3/2}$ states, respectively, with an energy difference of 2.7 eV indicating the presence of Nb_2O_5 [23]. The peak positions for all other samples are nearly the same with an energy difference of 2.7 eV. The results indicate formation only of Nb_2O_5 oxides for all the samples. It further confirms complete oxidation of Nb atom/molecules during reactive sputtering due to the absence of any peak corresponding to binding energy of Nb metal. The hump in the binding energy of O 1s has been deconvoluted into two peaks as shown in Fig. 4b. The peak at ~ 530 eV corresponds to Nb–O bond, whereas the one at 532 eV is due to the presence of non-lattice oxygen in the film [24]. Signature of non-lattice oxygen in all the films is confirmed from the XPS spectra. The non-lattice oxygen content in all the films is depicted in Table 3. The percentage of non-lattice oxygen represents the percentage of oxygen vacancies (V_O) [25] that increases with increasing oxygen concentration up to a certain value beyond which it decreases. In other words, the lattice oxygen percentage decreases with increasing oxygen content beyond a certain oxygen concentration in the plasma, i.e., up to 40% in this case. The deposited film at lower oxygen content removes the oxygen defects and produces more lattice oxygen (Nb–O lattice) [26]. At higher oxygen flow rates, the system prefers to form stoichiometric Nb_2O_5. Above 40% oxygen content of the plasma, the film composition remains constant and the oxygen content does not have any significant influence on the stoichiometry of the film.

The resistive switching properties of $Al/Nb_2O_5/Si$ devices are depicted in Fig. 5. The voltage was swept across the devices following a sequence 0→ -20 → +20 → 0 V, and the gate current was measured. Current change of three to five orders is observed for all the devices in the negative cycle of the voltage sweep. The SET voltages for N1, N2, N3, and N4 devices are −17.5 V, −16.4 V, −11 V, and −9.4 V, respectively. The devices change from high-resistance state (HRS) to low-resistance state (LRS) at a certain threshold negative voltage bias. Thus, the SET process is attained. When the voltage sweeps from negative to positive direction, it shows hysteresis indicating slow removal of charges upon reverse voltage sweep to achieve the RESET state. Upon perusal of the film thickness and SET voltage data, it is seen that the electric field at which the SET process took place is ~ 3 MV/cm.

The resistive switching behaviors of the MOS devices may be explained on the basis of porosity [27] and presence of non-lattice oxygen in Nb_2O_5 film. It is revealed from EDP profile in Fig. 2a that N1 samples are denser, whereas the rest samples exhibit comparable porosity. As shown in Fig. 5a, N1 device offers the poorest performance, whereas N3 shows better device performance than the other devices. Analysis of XPS data confirms that N3 device contains relatively more oxygen vacancies. It is seen earlier that the oxygen vacancies in the insulating oxide layer directly affect the memory properties of the device [24].

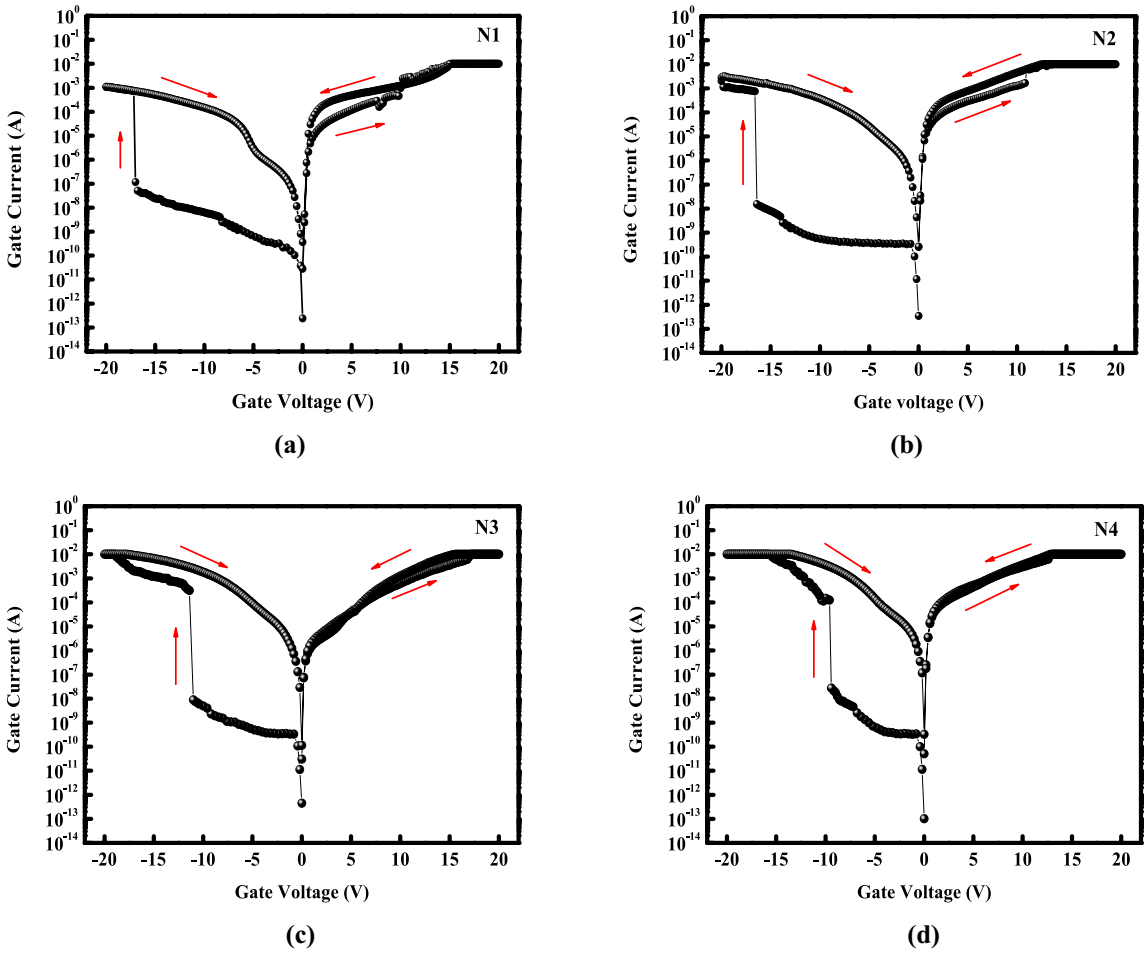

Fig. 5 Room temperature $I - V$ plots of the devices: **a** N1, **b** N2, **c** N3, and **d** N4

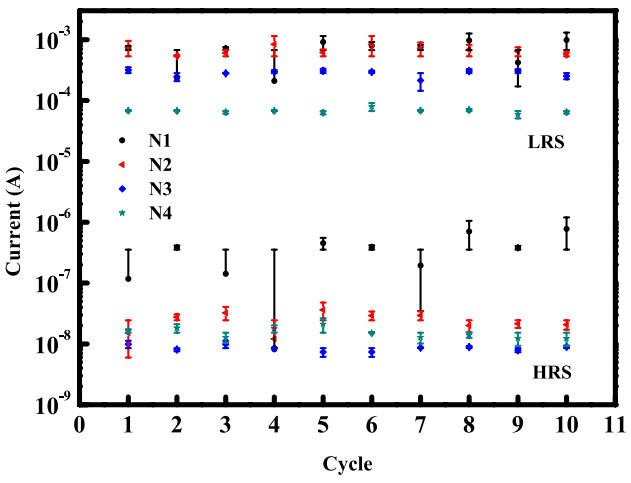

Fig. 6 Variation of current at HR and LR states with number of cycles. Error bars in the figure denote deviation from the mean value

Figure 6 shows the cycle-to-cycle variation of LRS and HRS current. Device with higher oxygen concentration in sputtering chamber gives better uniformity in current distribution. A five-order on/off ratio has also been observed using MOS structure, whereas the same order is also reported with MIM devices [18].

The whole phenomena may be explained on the basis of oxygen filament theory. When a negative voltage sweep is applied to the top metallic Al electrode, oxygen ions present in the Nb_2O_5 layer are pushed toward the bottom silicon. The accumulation of oxygen vacancies (V_O) is induced at the interface between top electrode and oxide layer. At a certain negative voltage, the forming process is finally completed creating a V_O-based conducting filament connecting the top and bottom electrodes. This CF forms a conduction path for electrons to travel from Al gate to the silicon substrate. The device then readily attains its LRS. In the reset process, the oxygen vacancies merge with the oxygen ions, thereby breaking the conductive filament. From the XRR data, it is evident that the porosity of N2, N3, and N4 samples shows nearly the same value. But the

XPS data reveal more non-lattice oxygen content in the N3 film. The porosity in the film generates defects during sputtering, and the defects in the thin film contribute to trap sites. When a critical number of traps are filled, a sudden increase in the magnitude of current is observed. Therefore, a critical porosity along with non-lattice oxygen content is required to get large swing in the resistive switching behavior of the Nb_2O_5-based MOS devices. In other words, N3 exhibits larger HRS/LRS implying a combined role of porosity and non-lattice oxygen on the RS device performance.

4 Conclusion

Nb_2O_5 films, deposited using reactive dc sputtering at different O_2/Ar ratios on Si substrate, have been characterized by X-ray photoelectron spectroscopy and X-ray reflectivity techniques. Metal–oxide–semiconductor devices were later fabricated with aluminum as top metal electrode with Nb_2O_5 film as gate dielectric. A dependence of the switching properties on the porosity of the films is evident. Further, the non-lattice oxygen content in the film also plays a role in determining the on/off ratio of the devices. Therefore, it is concluded that both film porosity and presence of non-lattice oxygen determine the switching behavior of the Nb_2O_5-based devices.

Acknowledgements The authors wish to acknowledge Prof. Mrinmay Mukhopadhyay and Prof. Manabendra Mukherjee, Saha Institute of Nuclear Physics (SINP), for providing the X-ray and AFM facilities, respectively. The contribution of Dr. Ramakrishnadeb Das, SINP, for X-ray data acquisition is also gratefully acknowledged. One of the authors Mr. Karimul Islam also acknowledges the financial assistance received from the University Grants Commission.

Compliance with ethical standards

Conflicts of interest On behalf of all authors, the corresponding author states that there is no conflict of interest.

References

1. Goux L, Lisoni JG, Jurczak M, Wouters DJ, Courtade L, Muller C (2010) Coexistence of the bipolar and unipolar resistive-switching modes in NiO cells made by thermal oxidation of Ni layers. J Appl Phys 107:024512
2. Lin CY, Wua CY, Wua CY, Hub C, Tseng TY (2007) Bistable resistive switching in Al_2O_3 memory thin films. J Electrochem Soc 154:G189
3. Goux L, Czarnecki P, Chen YY, Pantisano L, Wang XP, Degraeve R, Govoreanu B, Jurczak M, Wouters DJ, Altimime L (2010) Evidences of oxygen-mediated resistive-switching mechanism in TiN/HfO_2/ Pt cells. Appl Phys Lett 97:243509
4. Parreira P, Paterson GW, Mcvitie S, MacLaren DA (2016) Bistability and instability of amorphous ZrO_2 resistive memory devices. J Phys D 49:095111
5. Salaoru I, Prodromakis T, Khiat A, Toumazou C (2013) Resistive switching of oxygen enhanced TiO_2 thin-film devices. Appl Phys Lett 102:013506
6. Hiatt WR, Hickmott TW (1965) Bistable switching in niobium oxide diodes. Appl Phys Lett 6:106
7. Halbritter J (1987) On the oxidation and on the superconductivity of niobium. Appl Phys A 43:1
8. Jung K, Kim Y, Im H, Kim H, Park B (2011) Leakage transport in the high-resistance state of a resistive-switching NbO_x thin film prepared by pulsed laser deposition. J Korean Phys Soc 59:2778
9. Nico C, Monteiro T, Graça MPF (2016) Niobium oxides and niobates physical properties: review and prospects. Prog Mater Sci 80:1
10. Venkataraj S, Drese R, Kappertz O, Jayavel R, Wuttig M (2001) Characterization of niobium oxide films prepared by reactive dc magnetron sputtering. Phys Stat Solidi 188:1047
11. Im H, Pashkin YuA, Yamamoto T, Astafiev O, Nakamura Y, Tsai JS (2006) Characterization of ultrasmall all-Nb tunnel junctions with ion gun oxidized barriers. Appl Phys Lett 88:112113
12. Petrucci M, Pitt CW, Reynolds SR, Milledge HJ, Mendelssohn MJ, Dineen C, Freeman WG (1988) Growth of thin-film niobium and niobium oxide layers by molecular-beam epitaxy. J Phys Lett 63:900
13. Jung K, Kim Y, Jung W, Im H, Park B, Hong J, Lee J, Park J, Lee J-K (2010) Electrically induced conducting nanochannels in an amorphous resistive switching niobium oxide film. Appl Phys Lett 97:233509
14. Maruyama T, Arai S (1993) Electrochromic properties of niobium oxide thin films prepared by radio-frequency magnetron sputtering method. Appl Phys Lett 63:869
15. Hunsche B, Vergöhl M, Neuhäuser H, Klose F, Szyszka B, Matthee T (2001) Effect of deposition parameters on optical and mechanical properties of MF- and DC-sputtered Nb_2O_5 films. Thin Solid Films 392:184
16. Park J, Hadamek T, Posadas AB, Cha E, Demkov AA, Hwang H (2017) Multi-layered NiOy/NbOx/NiOy fast drift-free threshold switch with high Ion/Ioff ratio for selector application. Sci Rep 7:4068
17. Herzig M, Weiher M, Ascoli A, Tetzlaff R, Mikolajick T, Slesazeck S (2019) Improvement of NbOx-based threshold switching devices by implementing multilayer stacks. Semicond Sci Technol 34:075005
18. Deswal S, Kumar A, Kumar A (2018) Investigating unipolar switching in Niobium oxide resistive switches: correlating quantized conductance and mechanism. AIP Adv 8:085014
19. Kern W (1990) The evolution of silicon wafer cleaning technology. J Electrochem Soc 137:1887
20. Jagannath UK, Goutam RK, Sharma J, Singh K, Dutta US, Sule R, Pradeep SC (2018) Gadkari, HAXPES beamline PES-BL14 at the Indus-2 synchrotron radiation source. J Synchrotron Rad 25:1541–1547
21. Parrat LG (1954) Surface studies of solids by total reflection of X-rays. Phys Rev 95:359
22. Kundu S, Hazra S, Banerjee S, Sanyal MK, Mandal SK, Chaudhuri S, Pal AK (1998) Morphology of thin silver film grown by dc sputtering on Si(001). J Phys D Appl Phys 31:L73
23. özer N, Rubin MD, Lampert CM (1996) Optical and electrochemical characteristics of niobium oxide films prepared by sol-gel process and magnetron sputtering a comparison. Sol Energy Mater Sol Cells 40:285
24. He P, Ye C, Wu J, Wei W, Wei X, Wang H, Zhang R, Zhang L, Xia Q, Wang H (2017) Effect of sputtering atmosphere on the

characteristics of ZrOx resistive switching memory. Semicond Sci Technol 32:7
25. Chang YC, Lee KJ, Lee CJ, Wang LW, Wang YH (2016) Bipolar resistive switching behavior in sol-gel $MgTiNiO_x$ memory device. IEEE J Electron Devices Soc 4:321
26. Salunkhe P, Ali M, Kekuda D (2020) Investigation on tailoring physical properties of Nickel Oxide thin films grown by dc magnetron sputtering. Mater Res Express 7:016427
27. Fan Y, King S, Bielefeld J, Orlowski M (2016) Characterization of porous BEOL dielectrics for resistive switching. ECS Trans 72:35